



THE UNIVERSITY *of* EDINBURGH

Edinburgh Research Explorer

The conserved sonic hedgehog limb enhancer consists of discrete functional elements that regulate precise spatial expression

Citation for published version:

Lettice, LA, Devenney, PS, De Angelis, C & Hill, RE 2017, 'The conserved sonic hedgehog limb enhancer consists of discrete functional elements that regulate precise spatial expression', *Cell Reports*, vol. 20, no. 6, pp. 1396-1408. <https://doi.org/10.1016/j.celrep.2017.07.037>

Digital Object Identifier (DOI):

[10.1016/j.celrep.2017.07.037](https://doi.org/10.1016/j.celrep.2017.07.037)

Link:

[Link to publication record in Edinburgh Research Explorer](#)

Document Version:

Peer reviewed version

Published In:

Cell Reports

General rights

Copyright for the publications made accessible via the Edinburgh Research Explorer is retained by the author(s) and / or other copyright owners and it is a condition of accessing these publications that users recognise and abide by the legal requirements associated with these rights.

Take down policy

The University of Edinburgh has made every reasonable effort to ensure that Edinburgh Research Explorer content complies with UK legislation. If you believe that the public display of this file breaches copyright please contact openaccess@ed.ac.uk providing details, and we will remove access to the work immediately and investigate your claim.



The conserved sonic hedgehog limb enhancer consists of discrete functional elements that regulate precise spatial expression.

Laura A Lettice, Paul Devenney, Carlo De Angelis, and Robert E Hill*

MRC Human Genetics Unit, MRC Institute of Genetics and Molecular Medicine,
University of Edinburgh, Edinburgh, United Kingdom EH4 2XU

*Corresponding author and lead contact:

Robert Hill

MRC Human Genetics Unit
MRC Institute of Genetics and Molecular Medicine
University of Edinburgh
Edinburgh, United Kingdom EH4 2XU

Email Bob.Hill@igmm.ed.ac.uk

Phone +44-(0)131-6518621

SUMMARY

Expression of sonic hedgehog (*Shh*) in the limb bud is regulated by an enhancer called the ZRS, which in evolution belongs to an ancient group of highly conserved *cis*-regulators found in all classes of vertebrates. Here, we examined the endogenous ZRS in mouse using genome editing to establish the relationship between enhancer composition and embryonic phenotype. We show that enhancer activity is a consolidation of distinct activity domains. Spatial restriction of *Shh* expression is mediated by a discrete repressor module; whereas, levels of gene expression are controlled by large overlapping domains containing varying numbers of HOXD binding sites. The number of HOXD binding sites regulate expression levels incrementally. Substantial portions of conserved sequence are dispensable indicating the presence of sequence redundancy. We propose a collective model for enhancer activity in which function is an integration of discrete expression activities and redundant components that drive robust expression.

Key Words: *Shh* expression, limb development, ZRS, enhancer, *HoxD* genes, Werner mesomelic syndrome, genome editing, phenotype

Highlights

- The ancient vertebrate enhancer, the ZRS, shows sequence plasticity.
- Discrete regulatory activities are assigned to specific sites in the enhancer.
- Number of HOXD binding sites determines the level of *Shh* expression.
- Robust expression is a collective of regulatory and redundant information.

52 In brief (eTOC)

53 Lettice et al. examine the composition of a highly conserved limb-specific enhancer,
54 the ZRS, by dissecting the endogenous sequence using genome editing. Analysis of the
55 resulting phenotype gives insights into the complex composition of the enhancer which
56 integrates discrete expression activities and redundant elements to drive accurate
57 spatiotemporal gene expression.

58

59

INTRODUCTION

The basis of embryonic development lies in the spatiotemporal control of gene expression, which is mediated by remote *cis*-regulatory elements. These *cis*-acting elements, or enhancers, are fundamental to evolution and disease. Despite these important roles, major unanswered questions remain about the information encoded by the enhancer sequence and the importance of the overall structural architecture to enhancer activity. One class of enhancers that operates during embryogenesis are those that are highly conserved acting at long distances from their target genes (Visel et al., 2009). Here, we focus on a highly conserved element called the ZRS that is responsible for the spatiotemporal expression of *Shh* during limb bud development (Lettice et al., 2003; Sagai et al., 2005) and is essential for specifying digit identity and number. This enhancer is ~770bp in length and shows a high degree of similarity in vertebrates across a lengthy evolutionary time scale including the sharks and rays (Dahn et al., 2007) and in accord, the mouse shows >70% similarity with the coelacanth (lobe finned fish) sequence (Fig. S1). Hence, the ZRS has remained highly invariant against a backdrop of major evolutionary changes to the anatomy of the appendicular skeleton which includes the transition of fish fins to tetrapod limbs (Gehrke and Shubin, 2016). The structural organisation of this class of deeply conserved vertebrate enhancers is under strong selective constraints and even in light of binding site redundancies exhibited by transcription factors few sequence changes are present.

The ZRS is located 800-1000 kb away from the *Shh* promoter in mouse and human and is necessary and sufficient for accurately activating and maintaining *Shh* expression in the limb (Lettice et al., 2003; Sagai et al., 2005). An enhancer evolves not simply as a regulator that switches gene expression on or off but must also solve the challenges of

regulating expression from a distance (Lettice et al., 2014) while controlling gene activity accurately in space and time and at the appropriate levels. Based on the evolutionary stasis of the ZRS, it is reasonable to expect that the sequence was finely honed during evolution such that there is little tolerance for sequence change. Indeed point mutations in and duplications of the ZRS result in a spectrum of appendicular skeletal defects (Anderson et al., 2012). Point mutations in well over 20 different positions scattered across the ZRS cause autosomal dominant limb defects, called 'ZRS associated syndromes' (Wieczorek et al., 2010). Some of the conditions associated with ZRS mutations include preaxial polydactyly type 2, triphalangeal thumb polysyndactyly, syndactyly type 4 and Werner mesomelic syndrome (WMS).

To investigate the structural composition of this highly conserved vertebrate enhancer, we used genome editing technology (Dow, 2015) to target deletions in three regions within the ZRS. Since ZRS activity is limb specific, the phenotypes were expected to be overt, accessible and nonlethal. The regions that were targeted contain the 5bp site responsible for Werner's mesomelic syndrome (Anderson et al., 2012), the single mutation responsible for hemimelic extra toes (*Hx*) (Lettice et al., 2008) in mouse and a previously identified site for binding the HAND2 transcription factor (Osterwalder et al., 2014). This approach generated an overlapping series of mutations and deletions that scan across 250bp of the endogenous ZRS. Here, we show that the ZRS encodes multiple, diverse functions that contribute to the enhancer activity. Spatial restriction of expression is, in part, controlled by a small repressor domain which confines Shh expression to the posterior limb bud margin. In contrast, large overlapping domains regulate expression levels contingent on the number of HOXD binding sites. In addition, in response to insertion mutations cryptic, unique phenotypes were generated that revealed the functional plasticity

potentially encoded in an enhancer. Mutational analysis, however, also showed that even though the enhancer is highly conserved it could still tolerate quite substantial losses of sequence information without causing an abnormal phenotype. We propose a collective model for enhancer composition in which discrete activities and redundant sequences in the ZRS accrue to provide for a robust regulatory response during development.

RESULTS

ZRS Mutations in Mouse Mimics Werner Mesomelic Syndrome

The Werner mesomelic syndrome (WMS) is associated with point mutations in a single, short 5 bp stretch of the ZRS (green box, Fig. 1A) which results in preaxial polydactyly of the hands and feet but is uniquely associated with short limb dwarfism due to tibial hypoplasia. WMS results from any heterozygous point mutation at position 404 (in human) (Fig. 1A) (Lettice et al., 2008), a heterozygous A to G change two nucleotides downstream at position 406 (Norbnop et al., 2014) and a homozygous C to T change at position 402 (VanderMeer et al., 2014) (Green bases in Fig. 1A). These three nucleotide positions lie within a highly conserved site and to date is the only site association with this syndrome.

Initially, to examine the nature of these mutations in mouse and to ensure that it is possible to recreate the human abnormality, a G to A replacement in position 404 originally reported in a Cuban family (labelled as Cu; Fig.1A) (Lettice et al., 2003) was generated in mouse using conventional 'knock-in' technology (Lettice et al., 2014). The resulting heterozygous mice exhibited extra preaxial digits on the hindlimbs (Fig.1C) while homozygotes, in addition, had bent legs due to tibial dysplasia (Fig. 1D). Bone stains confirmed the loss of the terminal portion of each tibia (Fig. 1D), which copied the dysplastic

tibias of the WMS patients; however, unlike the patients the forelimbs in mice were unaffected and tibia dysplasia only occurred in the homozygous mutant.

To investigate further the nature of the dominant mutations at the WMS position, we targeted deletions using CRISPR/Cas9. A guide RNA (gRNA) targeted to this region (black box in Fig. 1A) resulted in a number of different deletions and insertions. The most common mutation that was recovered was the precise removal of the five basepairs (called the WMS Δ 5 deletion) (Green box in Fig. 1A) implicated as the site of WMS. The hindlimb phenotype of the WMS Δ 5 mutant mice is similar to that observed in the homozygous Cu mutant mice; in that, the hind limbs show extra preaxial digits and the tibia is hypoplastic ranging from a partial loss of the distal portion of the bone to its complete absence (Fig. 1E). In contrast to the point mutation, these phenotypes occurred in both heterozygous and homozygous WMS Δ 5 mice and both genotypes exhibit PPD in the forelimbs (Fig. 1F). Thus the strength of the WMS Δ 5 allele is similar to the point mutation in human. No differences in the severity of the phenotypes were observed between heterozygous and homozygous mice.

Analysis of *Shh* expression in the developing limb buds in the homozygous Cu mutant embryos showed normal expression at E10.5, while by E11.5 ectopic anterior expression of *Shh* (Fig. 1I) was observed in approximately half of the embryos examined (3/7 mice). By E12.5, ectopic *Shh* occurred at the anterior margin (Fig. 1J) in an outgrowth of limb tissue in all embryos examined. Heterozygous embryos showed normal *Shh* expression at all stages examined but analysis of *Ptc1*, a sensitive readout of *Shh* signalling, showed ectopic, anterior expression at both E11.5 and E12.5 (Fig. 1K, L) showing that low but sufficient levels of ectopic *Shh* were present in all mutant limb buds at these stages. Both heterozygous and homozygous WMS Δ 5 mutant embryos showed appreciably more *Shh* and *Ptc* expression at

the ectopic site of the hind limb bud at E11.5 (Fig. 1M, N) than detected in the homozygous Cu embryos, with some also showing ectopic expression in the fore limbs. Thus, the levels of ectopic *Shh* signalling detected reflected the final phenotype with long bone abnormalities arising in those limb buds expressing higher levels of ectopic *Shh* earlier in development. The clustering of the human mutations within a short 5bp sequence causing WMS indicates that this is a single important site for transcription factor binding; while, the deletions confirm that WMS is due to the loss of binding of a repressor that actively represses ectopic expression.

Small Insertions Extend the Limb Phenotypic Spectrum

A second set of mutations arose adjacent to the 5bp WMS site resulting in the insertion of either one or two additional adenosines (called +A and +AA in Fig. 2A). The mutant phenotype generated in the WMS+A mutant heterozygotes was a lengthening of the first digit and sometimes the addition of an extra terminal phalange on digit 1 of the hind limbs (Fig. 2B) with normal fore limbs. *Shh* expression appears normal in +A mutant limb buds at E11.5 (Fig. 2C); however, the phenotype suggests a low level of expression at the ectopic, anterior margin of the limb bud. Insertion of +AA resulted in a more severe phenotype which has not been previously described for ZRS associated mutations. This dinucleotide insertion caused typical PPD in the fore limbs (Fig. 2D) but in the hind limbs extra digits occurred centrally in the digital array (Fig 2E), occasionally in conjunction with long bone anomalies (1 in 7 heterozygotes) (Fig. 2F). The +AA hind limb buds showed an extended pattern of ectopic expression covering from the posterior margin all around the distal edge of the limb bud (Fig.2G). The plasticity of a developmental enhancer in producing morphological changes has been investigated in *Drosophila* (Swanson et al., 2010) and in mouse, it is clear that point mutations in the ZRS give rise to additional preaxial digits

and to homeotic transformations of the thumb to a finger (Anderson et al., 2012). The +AA mutant embryo presents an unusual skeletal configuration in the digital ray indicating that further cryptic plasticity is uncovered by mutational events that disrupt the enhancer's organization.

Large Regions within the ZRS are Dispensable

We next focussed our mutation analysis on two highly conserved regions 3' of the WMS site (Fig. 3A, see Fig. S1 for sequence comparison) to delve into the function of previously identified sites that are putatively important for *Shh* gene regulation. Corresponding gRNAs were designed that overlapped these sites (sequences shown as boxes in Fig.3B and J, with the PAM sites in italics). One region contains the conserved E-box that binds the transcription factor HAND2 (Osterwalder et al., 2014) (Fig. 3A, and blue nucleotides in 3B) crucial to the spatial specific activation of *Shh* in the posterior margin of the limb bud. The second region contains the *Hx* mouse point mutation which lies at position 553 (Fig.3A and red nucleotide in 3J) shown by transgenic analysis to operate as a dominant gain-of-function mutation and to encode important structural features crucial for enhancer activity (Lettice et al., 2014). In addition, the *Hx* site is embedded in a large region of the enhancer that is crucial for the long-range activity of the enhancer.

A series of overlapping deletions targeting the Ebox were identified (Fig. 3B), two of these disrupted the Ebox; Ebox Δ 3 which was Ebox specific removing the 3 nucleotides from the middle, and Ebox Δ 17 which deleted the Ebox and surrounding nucleotides. Two other deletions Ebox Δ 8 and Ebox Δ 16 removed nucleotides at the 3' side of the Ebox. None of these four deletions showed a phenotype either as heterozygotes or homozygotes (number of homozygotes analysed shown as n=, in Fig. 3B) For example, the largest deletion, Ebox Δ 17, which disrupts the Ebox and removes surrounding nucleotides showed wildtype

skeletal patterns in both the fore and hind limbs (Fig. 3C and D, respectively). *Shh* expression in the limb buds for all four deletions showed the normal posterior pattern in homozygous embryos (Fig. 3F-I). The Ebox Δ 3 and Ebox Δ 17 deletions suggest that removal of a single Ebox site has no detectable effect on *Shh* expression. Possibly, a second conserved Ebox site downstream which has a lower affinity for HAND2 (Osterwalder et al., 2014) may compensate for this loss. The Ebox Δ 8, Ebox Δ 16 and Ebox Δ 17 mutations overlap in a conserved region (Fig. 3B and S1) deleting a total of 24bp. No deletions in this region affected the limb phenotype showing that a substantial region of conserved information can be disrupted.

Using gRNA targeted to the *Hx* mutation, we identified four deletions, 3' Δ 42, 3' Δ 11, 3' Δ 12, and 3' Δ 8, all of which are encompassed in 56bp including the *Hx* site (Fig. 3J) and none of these had an effect on limb phenotype. Similar to the deletions created for the Ebox, these removed highly conserved nucleotide stretches; the 3' Δ 8 and Δ 12 deletion disrupting a HOXD binding site (Hoxsite 4, orange nucleotides in Fig 3J, and Fig. 5) (see below). The 3' Δ 11 and 3' Δ 42 remove the *Hx* mutant site and no polydactylous phenotype is detected in the heterozygotes confirming that, unlike the WMS mutations, the *Hx* point change is a gain-of-function mutation (Lettice et al., 2014). The two other deletions, 3' Δ 8 and 3' Δ 12, do not contain the *Hx* mutant site but do remove the adjacent highly conserved sequences containing the Hoxsite4 and these do not show a heterozygous phenotype. Homozygous mutants were made for all these deletions and no phenotype was detected (*n* numbers are shown in Fig. 3J). The larger 127 bp deletion (3' Δ 127) (Fig. 3A and S1) confirmed this tolerance for loss of conserved sequence. The large 3' Δ 127 allele, showed no dominant effect on digit number and in the homozygous state there was no influence on the limb phenotype (*n*=7) (Fig. 3K, L) while both *in situ* hybridization and qRT-PCR showed no

appreciable change in the expression profile or levels (Fig. 3M, N). This deletion showed that a large region of conserved sequence can be deleted from this enhancer. Since the mutational analysis was performed at the endogenous locus, the lack of a phenotype suggests that the loss of the 3' Δ 127 sequence is compensated for; thus, indicating that there is encoded redundancy within the enhancer.

Large Deletions Encompassing the WMS Site Incrementally Affect Expression Levels

Three other deletions were generated (FIG. 4A, Fig S1) when making the WMS mutations; a 20bp deletion, WMS Δ 20, which included the 5bp site of the WMS Δ 5 and two other deletions, WMS Δ 48 and WMS Δ 110; both of which lost 21bp on the 3' side of the WMS site removing the E-box element but extending to different positions at the 5' end. The WMS Δ 20 deletion, unexpectedly showed no observable limb phenotype; neither a dominant phenotype displaying extra toes nor in the WMS Δ 20/WMS Δ 20 homozygote, a loss of activity phenotype displaying skeletal deficiencies ($n=5$) (Fig. 4B, C). The WMS Δ 20 mouse was further crossed to the *Shh* null mutation to make the WMS Δ 20/*Shh*^{null} compound heterozygote to expose any subtle loss of activity but these again, showed no abnormal phenotype ($n=5$). Analysis of *Shh* expression in WMS Δ 20 homozygotes showed little observable differences in the expression pattern (Fig. 4H) compared to wildtype (Fig. 4K) and levels of expression measured by qRT-PCR were not affected significantly (Fig. 4L). Thus the deleterious phenotypic effects of the WMS Δ 5 mutations were lost in the larger WMS Δ 20 deletion.

The two deletions, WMS Δ 48 and WMS Δ 110 (FIG. 4A), were examined and in the homozygote removal of these sequences resulted in loss of digits. The WMS Δ 48 mutation showed loss of up to one digit on each on the forepaws (Fig. 4D), with some elements being retained and soft and hard tissue syndactyly and fusion being observed. The hindpaws were

mildly affected, some showing only partial loss of a single digit (digit 3) (Fig.4E). The WMS Δ 110 embryos showed a precise loss of one digit on all four paws (Fig. 4F, G), with the rest of the digits apparently unaffected. Since these phenotypes were seen only in the homozygous state, these were loss of activity mutations resulting in a decrease in enhancer activity. Indeed *Shh* expression was lower but was retained at the posterior margin of the limb bud at E11.5 but by *in situ* hybridisation levels in Δ 48 (Fig. 4I) appeared appreciably lower than wildtype (Fig. 4K), with further reductions in the WMS Δ 110 (Fig. 4J). Levels of RNA measured by qRT-PCR showed a significant reduction in *Shh* both WMS Δ 110 and WMS Δ 48 compared to wildtype (Fig. 4L).

Multiple, Conserved HOX Binding Sites Control Expression Levels of *Shh*

Within the ZRS, a highly conserved 6bp element composed of the sequence CATAAA was detected at four positions (boxed in Fig. 5, FigS1). This 6bp sequence is embedded in sites that compare well to the consensus motif established for the 5' *Hoxd* genes (motif for HOXD9-11 shown Fig. 5,) and these were numbered Hoxsites 1-4. Genetic analysis of the HOX complexes previously demonstrated that the 5' *Hoxd* genes (*Hoxd*10-13) and their counterparts in the *Hoxa* locus regulate *Shh* expression in the limb (Tarchini et al., 2006) and chromatin immunoprecipitation (ChIP) showed that at least two Hox proteins, HOXD10 and 13, directly bind to the ZRS (Capellini et al., 2006). Three of these identified sites (Hoxsites1, 2 and 3) are contained within the Δ 110 deletion, the Δ 48 contained two sites (Hoxsite2 & 3) and the Δ 20 contained only Hoxsite 3 (Fig. 5, FigS1). Hoxsite 4 was deleted in the series that included the *Hx* site (Fig. 3J) discussed above. Each of the 5' *Hoxd* genes was cloned into the vector pT7CFE1-CHis for subsequent expression in the human *in vitro* expression system (1-Step Human Coupled IVT Kit, Thermo Fisher Scientific). The 5' HOXD proteins were synthesised (Fig. S2) and used in an electromobility shift assay (EMSA) to establish binding

to double-stranded oligonucleotides containing one of these four sites (Table S1). The *in vitro* synthesized HOXD9, 10, and 11 proteins showed the highest binding activity with these sites (Fig. 5) while HOXD12 and 13 showed lower activity across all oligos (Fig. S2B). The HOXD proteins showed different preferences for these sites; HOXD9 and 11 bound all four sites, with D9 showing a preference for sites 3 and 4 while D11 favoured Hoxsites 1, 2 and 3. HOXD10 bound site 3 but bound weakly to Hoxsites 1, 2 and 4 (Fig. 5). Specificity of binding was shown using competitor oligonucleotides with either wildtype sequence or Hox binding site mutations (Fig 5, Table S1). Nuclear extracts from embryonic (E11.5) limb buds were also used in EMSA (Fig. 5) and was found to bind to all sites and the binding was specific for the putative HOX binding motif.

The role played by the three HOX sites (Hoxsites 1-3) contained in the Δ 110 deletion on ZRS activity was assayed in a series of transgenic embryos. Each site was mutated by replacing three bases in the CATAAA element (mutations for each site shown in Fig. 6A) in a construct carrying the mutated, full-length ZRS driving the expression of a *LacZ* reporter gene. Mutations in each of these HOXD binding sites were made individually or in combination and expression was examined at E11.5 in each injected transgenic embryo (the transient G₀ embryo). As a measure of the relative extent of expression in each transgenic embryo, the width of expression as a percentage of limb bud width was plotted to show the trends (individual limbs are represented by dots in Fig. 6P). Mutations in individual Hoxsites had no observable effects on transgenic expression in the limb bud (in Fig. 6, compare B with C, D and E; Fig. 5P); however, mutations in the two sites (Hoxsites 2 and 3) that were contained in the Δ 48 deletion or mutations in Hoxsites 1 and 3 showed detectably decreased expression (Fig. 6F, G and P). Mutation of all three sites (Hoxsites 1-3) showed even further decreases (Fig. 6H and P) comparable to the ZRS carrying the Δ 110 deletion

(Fig. 6I and P). The accumulative decrease in expression of the endogenous *Shh* in the $\Delta 48$ and $\Delta 110$ deletions correlates with the progressive loss of the HOXD binding sites Hoxsites 1-3.

Deletions of the WMS Domain Restores the Wildtype Phenotype

The deletion in WMS $\Delta 20$ removes the WMS repressor site but also includes the Hoxsite 3. Transgenics carrying either the Cu point mutation (Lettice et al., 2003) (Fig. 6J) or the WMS $\Delta 5$ deletion (Fig. 6K) drives reporter gene expression to an elevated level in the posterior margin of the limb bud (Fig. 6P) with appreciable ectopic expression. The WMS $\Delta 20$ deletion appears to return transgenic expression to wildtype levels (Fig. 6L, P). The loss of the WMS repressor in combination with the mutant Hoxsite 3 binding site may be sufficient to nullify the increased and ectopic expression by the WMS mutations. To examine this possibility, transgenic mice carrying the Cu mutation in the presence of the three basepair replacement (see above) that disrupts Hoxsite 3 was used in the transgenic assay, and showed no detectable upregulation of the reporter at E11.5 and importantly, no ectopic expression (Fig. 6M, P). To show that the lack of ZRS upregulation was due to the independent action of the WMS mutations and loss of Hoxsite binding, transgenics carrying the Cu change and a different Hoxsite mutation (Hoxsite 2) also predominantly showed the wildtype pattern of expression (one out of five G₀ embryos retained ectopic expression) (Fig. 6N, P). Reductions in expression were shown in the presence of the WMS point mutation when two Hoxsites are mutated (Fig. 6O, P). The transgenic expression reflects the WMS $\Delta 20$ deletion suggesting that the WMS mutation, which affects the binding of a repressor, when in the presence of mutations that disrupt binding of an activator effectively cancel each other's activities giving rise to wildtype expression levels. The independent action of these opposing activities emphasize the combinatorial nature of elements that operate in the ZRS.

DISCUSSION

The aim of this study was to investigate the composition of a vertebrate enhancer that falls into the highly conserved class of elements (Ovcharenko et al., 2004). These vertebrate enhancers represent a class in which the structural architecture is under selective constraints resulting in apparent structural inflexibility in both the redundancy and the positioning of transcription factor binding motifs. These enhancers which range in size from 100bp to >1kb have the capacity to bind a substantial number of transcription factors arguing that within a single functional element there is also a degree of structural complexity. This structural complexity has enabled the dissection of the ZRS into discrete regulatory activities. The expression pattern of the *Shh* gene in the limb bud is a consolidation of activities that control restriction of expression to the posterior margin, spatial and temporal expression, levels of expression and long-range promoter activation (Summarised in Fig 7A).

Other examples of a complex arrangement of components have been reported including an elegant analysis of the *Drosophila spa* enhancer that showed structural organisation underlies correct developmental gene expression (Swanson et al., 2010); for instance, sequence elements were defined that regulate long range activity and the organization of other elements repress expression in the wrong cell type. Our analysis surveying deletions showed, further, a complex organization that included unexpected redundancy incorporated into the element. The model for enhancer action that we propose here is one that relies on consolidation of discrete, discernible activities acting as a collective. This collective model suggests an integration of these discrete activities and redundant elements in delivering robust spatiotemporal developmental expression.

Hox genes function at the ZRS to regulate levels of expression

We show the homotypic clustering of conserved HOXD binding sites (Hoxsites 1-4) in the ZRS. At least three of these sites (Hoxsites 1-3) are clustered in a 110bp domain of the ZRS and regulate levels of *Shh* expression. The 5'*HoxD* genes, which include *Hoxd 9-13*, are fundamental to limb patterning and are expressed in a temporal collinear fashion with the *Hoxd9* gene expressing earliest in the limb bud followed in sequence with *Hoxd13* being expressed latest (Tarchini and Duboule, 2006). A clustering of highly conserved sites that contain the core motif for binding the 5'HOXD proteins operate in an accumulative manner to regulate activity levels of the ZRS enhancer. In an *in vitro* assay, we showed that the early 5' HOXD proteins (HOXD9-11) bind this motif suggesting that these play an initial role in establishing the activity levels of the ZRS. The region of the ZRS that contains three of these HOXD motifs is crucial for activity and deletions show decreasing *Shh* expression corresponding to the number of Hox binding sites lost. In addition, loss of a Hox binding site counterbalances the increased and ectopic expression generated by the loss of the WMS repressor site. Thus, multiple HOXD factors coordinate, through the binding at multiple sites, the expression levels of *Shh*.

Additional HOXD binding sites have been identified near the 5' end of the ZRS which have a preference for binding HOXD13 (Leal and Cohn, 2016) (Fig 7B). Two sets of HOX sites, therefore, regulate gene expression reacting to the temporal changes in the expression of the 5'*Hoxd* genes. We suggest that the sites we identified play a role in establishing the levels of *Shh* expression in the initial stages of limb development by binding the early expressing 5'HOXD proteins (HOXD10, 11) but adjusts to the changing embryonic environment within the developing limb by also interacting with the later expressed HOXD13 at different sites.

This establishes a regulatory loop that operates by positive feedback, reinforcing the expression of the *Shh* gene by the 5'*HoxD* genes (Fig 7B). The early 5'HOXD proteins interact with the ZRS at the HOX binding sites examined in this study to establish the levels of *Shh* expression based on the sum of the sites occupied (Arrow 1, Fig.7B). SHH, in turn, is crucial for the shift in the regulation of *HoxD* gene expression from a set of early acting enhancers to the enhancers at the 5' end of the gene cluster (Arrow 2, Fig. 7B) that regulate the late expressing genes, in particular *Hoxd13* (Zákány et al., 2004). HOXD13 subsequently binds to sites at the 5' end of the ZRS established by Leal and Cohn (2016) (Arrow 3, Fig. 7B). We suggest that a temporal response to *HoxD* genes is important for continued *Shh* expression as the regulatory environment in the limb bud changes over the 2 days that *Shh* is expressed in the mouse limb.

In accord, the pythons and boa snakes which have lost the HOXD13 binding sites in the ZRS initially express *Shh* in the rudimentary limb buds, presumably dependent on the early 5'HOXD proteins binding sites that we established; however, *Shh* expression is lost later and limb development is prematurely terminated. This loss of the HOXD13 binding sites in combination with loss of an ETS binding site (Leal and Cohn, 2016; Kvon et al., 2016) is responsible for the loss of limbs in these snakes.

Homotypic clustering of binding sites in the ZRS appears to play a number of roles in determining the spatial expression pattern of *Shh* expression in the embryonic limb bud. We previously showed multiple binding sites for the ETS factors, ETS1 and GABP α (Lettice et al., 2012). Multiple occupancy of these sites determine the extent of the boundary of *Shh* expression. Mutations in the human ZRS which generate an extra ETS site results in the extension of this expression boundary and ectopic expression in the limb bud resulting in preaxial polydactyly (Lettice et al., 2012; Laurell et al., 2012). Here, occupancy of multiple

HOXD binding sites regulates the levels of expression, sequential loss of these sites result in a gradual decrease in expression levels. Homotypic clustering of binding sites in the ZRS, therefore, operates to adjust incrementally the expression of the *Shh* gene and is therefore, a fundamental mechanism for fine-tuning the regulatory activity of the enhancer.

ZRS Activity and Congenital Abnormalities

Mutations in the human ZRS cause skeletal abnormalities (Anderson et al., 2012). The point mutations act in a dominant fashion to cause digital abnormalities and presumably, most operate by switching restricted posterior expression to expression at both the posterior margin and an ectopic site at the anterior margin. One set of point mutations generates additional binding sites for ETS1/GABP α transcription factors, acting as dominant gain-of-activity mutations (Lettice et al., 2012). WMS, on the other hand, is highlighted by point mutations in three distinct positions in a single 5bp site. The action of these point mutations, confirmed by the WMS Δ 5 deletion data, is consistent with the loss of binding of a repressor and thus, an overall loss of functional activity. Hence, point mutations in ZRS have two modes of action, operating as both gain and loss of activity, but both resulting in dominant genetic effects on the phenotype.

Insertions Reveal Cryptic Phenotypes

The WMS+AA insertional mutation reveals an unusual phenotype showing the latent capacity for phenotypic innovation carried by this enhancer. The potential for appreciable morphological change shows that developmental enhancers may have the capacity for change without undergoing large sequence and structural changes in evolution. Selection against such substantial morphological changes may be one of the evolutionary constraints operating on the ZRS but, in contrast, this also highlights the capacity for appreciable change in vertebrate evolution. These additions reveal the plasticity that is potentially hidden

within an enhancer in controlling the phenotype and highlights mechanisms that may be available for phenotypic change during the evolution of an enhancer.

Evolution of the ZRS

The function of a *cis*-regulator is encoded in its molecular architecture. Overlapping deletions in the ZRS that would predictably disrupt this architecture were made near and encompassing the proposed E-Box binding site and the WMS site that removed a total of 44 basepairs of highly conserved sequence and these do not affect the limb phenotype. Moreover, the large 3'Δ127 mutation removes conserved sequence from the 3'half of the ZRS, which overlaps this 44bp and also displays neither a limb phenotype nor a detectable reduction in expression. The ability to compensate for loss of sequence information suggests that there is encoded redundancy within the enhancer. This seemingly redundant activity may contribute to phenotypic robustness during development. Robustness is deemed important to buffer developmental processes from environmental and genetic perturbations and was proposed as canalization by Waddington (Waddington, 1942). For enhancers, such redundancy is widespread in *Drosophila* (Cannavo et al., 2016). Secondary or 'shadow enhancers' in *Drosophila* provide redundant activity for the primary enhancer and analysis of specific examples show these can buffer a developmental process against environmental perturbations (Frankel et al., 2010; Perry et al., 2010). It is clear that the ZRS is able to tolerate losses of highly conserved sequence without affecting phenotype under ideal breeding conditions and defined genetic background. In contrast to shadow enhancers, the robustness apparent in the ZRS is encoded within a single enhancer element, since no compensatory activity is apparent in ZRS deletions. Hence, redundancy is an important characteristic of enhancers whether this is encoded in secondary enhancers or is contained within a single element such as in the ZRS.

The evolutionary stability of the ZRS sequence raises a number of questions about the evolvability of this, and perhaps other, highly conserved enhancers. In addition, this stability occurs in light of the major morphological changes that have occurred to the limb during vertebrate evolution. Thus the ZRS displays low sequence variability in a morphologically plastic developmental system. The recurrent role that the ZRS plays in the diverse species so far analysed is to ensure that *Shh* is expressed specifically along the posterior margin of the developing appendage whether it is an embryonic fin (Dahn et al., 2007) or a limb bud. Many of the genes and signalling pathways known to regulate *Shh* in mouse; such as the *HoxD* complex, *Hand2*, *Gli3* and the FGF pathway are implicated in chick and fish suggesting that the gene network responsible for *Shh* activation is also conserved (Gehrke and Shubin, 2016). For vertebrate enhancers, which are found in all vertebrate classes from cold-blooded fishes to warm-blooded mammals, it is unlikely that the apparent robustness is a response to environmental factors since these insults would be different for each species. The genetic network of transcription factors and signalling pathways that converge at the ZRS is complex and we suggest that the regulatory robustness observed for the ZRS buffers against variability and perturbations in this genetic network. This network that converges at the ZRS would, therefore, have evolved early in vertebrates operating relatively unchanged in the appendicular skeleton in all classes of vertebrates. The conserved enhancer architecture is a response to this complex network and would be a constant factor that pervades species evolution during the morphological changes that have occurred during the fin to limb transitions

EXPERIMENTAL PROCEDURES

Production and analysis of CrispR mice

Guide RNAs were designed using the Optimized CrispR design site (<http://crispr.mit.edu/>) and the exact guides chosen on the basis of their precise location relative to the desired sites in ZRS (Oligonucleotides selected are listed in Table S1). Oligos were cloned into px330 vector (Addgene) (Cong et al., 2013), and DNA prepared using Qiagen Plasmid Maxi kit (manufacturer's protocol).

Transgenic mice were made by pronuclear injection of plasmid DNA at a concentration of 5ng/μl. All resulting pups were screened phenotypically and had their ZRS sequence amplified by PCR and sequenced. All genotyping was performed by direct sequencing.

Skeletal preparations were stained simultaneously with Alizarin Red and Alcian Blue (Nagy et al., 2009a, b). Whole-mount *in situ* hybridisation was performed as previously described (Hecksher-Sorensen et al., 1998) using probes for *Shh* (Echelard et al., 1993) (a kind gift from Andy McMahon) and *Ptc* (Hayes et al., 1998) (a kind gift from Chris Hayes). qRT-PCR for *Shh* expression was performed on individual pairs of limb buds as described in Lettice et al., (2014). Expression was normalised within a litter to the wildtype level and statistical significance calculated by Prism using the Kruskal-Wallis test with Dunn's multiple comparisons. Mouse studies were approved by the University of Edinburgh AWERB and carried out under the auspices of the UK Home Office.

EMSAs/IVT proteins

The coding regions of mouse *Hoxd 9-13* were amplified by PCR using KOD polymerase (Merck Millipore). The primers used are listed in Table S1. Products were cloned into the expression vector pT7CFE1-CHis for subsequent expression in the human in vitro expression system (1-Step Human Coupled IVT Kit, Thermo Fisher Scientific) following the manufacturer's instructions. Synthesis of each of the HOXD proteins was verified on a

western blot using a rabbit anti-His Tag antibody (#2365, Cell Signalling Technology) (Fig. S2), before the protein was used in an electromobility shift assay (EMSA). The double stranded oligonucleotides were biotin labelled by the manufacturers (Sigma) and assayed to ensure that each was labelled to a similar specific activity. EMSAs were conducted as previously described (Lettice et al., 2012) and used either 2ul of a 1/25 dilution of protein from the IVT reaction or 4ug of limb bud extract (prepared using NE-PER® Nuclear and Cytoplasmic Extraction Reagent Kit, Thermo Scientific). The specificity of binding was confirmed by competition with 100x excess of either unlabelled wild type or mutant (mut) HoxSite oligonucleotides. (Table S1)

Mutant ZRS transgenic constructs

Reporter gene transgenic analysis were made as previously described (Lettice et al., 2012). The mutant ZRS deletions (WMS $\Delta 5$, $\Delta 20$, $\Delta 110$) used were generated by PCR using primers ZRSF and R (Table S1) from the appropriate mutant DNA. The Cu point mutation and MutHoxsite constructs were created using primers in Table S1 and a QuikChange II Site-Directed Mutagenesis Kit (Agilent). For combinations of sites, multiple rounds of mutagenesis were conducted and the correctly mutated ZRS subsequently cloned into fresh lacZ containing vector.

AUTHOR CONTRIBUTIONS

Conceptualization, L.L.; Methodology L.L., Validation L.L., Investigation L.L., P.D., C.D.; Writing – Original Draft R.H.; Writing – Review and editing L.L., R.H.; Visualization L.L.; Supervision L.L., R.H.; Funding Acquisition R.H.

ACKNOWLEDGEMENTS

We would like to thank Richard Mort for help with the statistical analysis and MRC Central Services for providing DNA sequence support. We would also like to thank the staff at the

515 Evans Building for expert technical assistance. Invaluable advice on the manuscript was
516 given by David Fitzpatrick, Nick Hastie and Wendy Bickmore. This work was supported by an
517 MRC core program grant.

518

519

520 **REFERENCES**

521 Anderson, E., Peluso, S., Lettice, L.A., and Hill, R.E. (2012). Human limb abnormalities
522 caused by disruption of hedgehog signaling. *Trends Genet* 28, 364-373.

523 Cannavo, E., Khoueiry, P., Garfield, D.A., Geeleher, P., Zichner, T., Gustafson, E.H., Ciglar,
524 L., Korbel, J.O., and Furlong, E.E. (2016). Shadow Enhancers Are Pervasive Features of
525 Developmental Regulatory Networks. *Curr Biol* 26, 38-51.

526 Capellini, T.D., Di Giacomo, G., Salsi, V., Brendolan, A., Ferretti, E., Srivastava, D.,
527 Zappavigna, V., and Selleri, L. (2006) Pbx1/Pbx2 requirement for distal limb patterning is
528 mediated by the hierarchical control of Hox gene spatial distribution and Shh expression
529 *Development* 133, 2263-73.

530 Cong, L., Ran, F.A., Cox, D., Lin, S., Barretto, R., Habib, N., Hsu, P.D., Wu, X., Jiang, W.,
531 Marraffini, L.A., et al. (2013). Multiplex genome engineering using CRISPR/Cas systems.
532 *Science* 339, 819-823.

533 Dahn, R.D., Davis, M.C., Pappano, W.N., and Shubin, N.H. (2007). Sonic hedgehog
534 function in chondrichthyan fins and the evolution of appendage patterning. *Nature* 445,
535 311-314.

536 Dow, L.E. (2015). Modeling Disease In Vivo With CRISPR/Cas9. *Trends Mol Med* 21, 609-
537 621.

538 Echelard, Y., Epstein, D.J., St-Jacques, B., Shen, L., Mohler, J., McMahon, J.A., and
539 McMahon, A.P. (1993). Sonic hedgehog, a member of a family of putative signaling
540 molecules, is implicated in the regulation of CNS polarity. *Cell* 75, 1417-1430.

541 Frankel, N., Davis, G.K., Vargas, D., Wang, S., Payre, F., and Stern, D.L. (2010). Phenotypic
 542 robustness conferred by apparently redundant transcriptional enhancers. *Nature* 466, 490-
 543 493.

544 Gehrke, A.R., and Shubin, N.H. (2016). Cis-regulatory programs in the development and
 545 evolution of vertebrate paired appendages. *Semin Cell Dev Biol.*

546 Hayes, C., Brown, J.M., Lyon, M.F., and Morriss-Kay, G.M. (1998). Sonic hedgehog is not
 547 required for polarising activity in the Doublefoot mutant mouse limb bud. *Development*
 548 125, 351-357.

549 Hecksher-Sorensen, J., Hill, R.E., and Lettice, L. (1998). Double labeling for whole-mount
 550 in situ hybridization in mouse. *Biotechniques* 24, 914-916, 918.

551 Kvon, E.Z., Kamneva, O.K., Melo, U.S., Barozzi, I., Osterwalder, M., Mannion, B.J.,
 552 Tissieres, V., Pickle, C.S., Plajzer-Frick, I., Lee, E.A., et al. (2016). Progressive Loss of Function
 553 in a Limb Enhancer during Snake Evolution. *Cell* 167, 633-642 e611.

554 Laurell, T., Vandermeer, J.E., Wenger, A.M., Grigelioniene, G., Nordenskjöld, A., Arner,
 555 M., Ekblom, A.G., Bejerano, G., Ahituv, N., and Nordgren, A. (2012) A novel 13 base pair
 556 insertion in the sonic hedgehog ZRS limb enhancer (ZRS/LMBR1) causes preaxial polydactyly
 557 with triphalangeal thumb. *Hum Mutat.* 33, 1063-6.

558 Leal, F. and Cohn, M.J. (2016). Loss and Re-emergence of Legs in Snakes by Modular
 559 Evolution of Sonic hedgehog and HOXD Enhancers *Curr Biol.* 26, 2966-2973.

560 Lettice, L.A., Heaney, S.J., Purdie, L.A., Li, L., de Beer, P., Oostra, B.A., Goode, D., Elgar, G.,
 561 Hill, R.E., and de Graaff, E. (2003). A long-range Shh enhancer regulates expression in the
 562 developing limb and fin and is associated with preaxial polydactyly. *Hum Mol Genet* 12,
 563 1725-1735.

564 Lettice, L.A., Hill, A.E., Devenney, P.S., and Hill, R.E. (2008). Point mutations in a distant
 565 sonic hedgehog cis-regulator generate a variable regulatory output responsible for preaxial
 566 polydactyly. *Hum Mol Genet* 17, 978-985.

567 Lettice, L.A., Williamson, I., Devenney, P.S., Kilanowski, F., Dorin, J., and Hill, R.E. (2014).
 568 Development of five digits is controlled by a bipartite long-range cis-regulator. *Development*
 569 141, 1715-1725.

570 Lettice, L.A., Williamson, I., Wiltshire, J.H., Peluso, S., Devenney, P.S., Hill, A.E., Essafi, A.,
 571 Hagman, J., Mort, R., Grimes, G., et al. (2012). Opposing functions of the ETS factor family
 572 define Shh spatial expression in limb buds and underlie polydactyly. *Dev Cell* 22, 459-467.

573 Nagy, A., Gertsenstein, M., Vintersten, K., and Behringer, R. (2009a). Alcian blue staining
 574 of the mouse fetal cartilaginous skeleton. *Cold Spring Harb Protoc* 2009, pdb prot5169.

575 Nagy, A., Gertsenstein, M., Vintersten, K., and Behringer, R. (2009b). Alizarin red staining
 576 of post-natal bone in mouse. *Cold Spring Harb Protoc* 2009, pdb prot5171.

577 Norbnop, P., Srichomthong, C., Suphapeetiporn, K., and Shotelersuk, V. (2014). ZRS
 578 406A>G mutation in patients with tibial hypoplasia, polydactyly and triphalangeal first
 579 fingers. *J Hum Genet* 59, 467-470.

580 Osterwalder, M., Speziale, D., Shoukry, M., Mohan, R., Ivanek, R., Kohler, M., Beisel, C.,
 581 Wen, X., Scales, S.J., Christoffels, V.M., et al. (2014). HAND2 targets define a network of
 582 transcriptional regulators that compartmentalize the early limb bud mesenchyme. *Dev Cell*
 583 31, 345-357.

584 Ovcharenko, I., Stubbs, L., and Loots, G.G. (2004). Interpreting mammalian evolution
 585 using Fugu genome comparisons. *Genomics* 84, 890-895.

586 Perry, M.W., Boettiger, A.N., Bothma, J.P., and Levine, M. (2010). Shadow enhancers
 587 foster robustness of *Drosophila* gastrulation. *Curr Biol* 20, 1562-1567.

588 Sagai, T., Hosoya, M., Mizushina, Y., Tamura, M., and Shiroishi, T. (2005). Elimination of a
 589 long-range cis-regulatory module causes complete loss of limb-specific Shh expression and
 590 truncation of the mouse limb. *Development* 132, 797-803.

591 Swanson, C.I., Evans, N.C., and Barolo, S. (2010). Structural rules and complex regulatory
 592 circuitry constrain expression of a Notch- and EGFR-regulated eye enhancer. *Dev Cell* 18,
 593 359-370.

594 Tarchini, B., Duboule, D., and Kmita, M. (2006) Regulatory constraints in the evolution of
 595 the tetrapod limb anterior-posterior polarity. *Nature* 443, 985-8.

596 Tarchini, B., and Duboule, D. (2006) Control of Hoxd genes' collinearity during early limb
 597 development *Dev Cell* 10, 93–103

598 VanderMeer, J.E., Lozano, R., Sun, M., Xue, Y., Daentl, D., Jabs, E.W., Wilcox, W.R., and
 599 Ahituv, N. (2014). A novel ZRS mutation leads to preaxial polydactyly type 2 in a
 600 heterozygous form and Werner mesomelic syndrome in a homozygous form. *Hum Mutat*
 601 35, 945-948.

602 Visel, A., Rubin, E.M., and Pennacchio, L.A. (2009). Genomic views of distant-acting
 603 enhancers. *Nature* 461, 199-205.

604 Waddington, C.H. (1942). Canalization of development and the inheritance of acquired
 605 characters. *Nature* 150, 563-565.

606 Wieczorek, D., Pawlik, B., Li, Y., Akarsu, N.A., Caliebe, A., May, K.J., Schweiger, B., Vargas,
 607 F.R., Balci, S., Gillessen-Kaesbach, G., et al. (2010). A specific mutation in the distant sonic
 608 hedgehog (SHH) cis-regulator (ZRS) causes Werner mesomelic syndrome (WMS) while
 609 complete ZRS duplications underlie Haas type polysyndactyly and preaxial polydactyly (PPD)
 610 with or without triphalangeal thumb. *Hum Mutat* 31, 81-89.

611 Zákány, J., Kmita, M., and Duboule, D. (2004). A dual role for Hox genes in limb anterior-
612 posterior asymmetry. *Science* 304, 1669-72.
613
614

Figure Legends

Figure 1. Mutational analysis of the WMS site in the ZRS. The position of the three sites within the ZRS that were targeted for mutation analysis are depicted in (A) and the WMS site is boxed. The conservation of the region containing the Werner mesomelic syndrome site is shown. The 3 nucleotides (green) mutated in WMS are shown in a green box and labelled WMS Δ 5, the Cu mutation is highlighted by the red box and the position of the gRNA is contained in the black box (the PAM site is underlined and in italics). The position of the +A and +AA insertion is also shown. The wildtype and mutant allele sequences are shown at the top of each panel. The wildtype hind limb (B) and expression patterns of *Shh* (G) and *Ptc* (H) at E11.5 hind limb buds are shown for comparison. The hindlimbs of the Cuban mutation (a G > A point change) shows an extra anterior digit in the heterozygote (C) and a polydactylous hindlimb and the hypoplastic tibia in the homozygote (D). *Shh* expression in the Cu homozygote at E11.5 (I) and E12.5 (J) and *Ptc* in the heterozygote at E11.5 (K) and E12.5 (L) are shown. Ectopic expression is highlighted by the black arrows. The heterozygous WMS Δ 5 deletion mutants are shown in (E, F, M and N). The hindlimb shows the absence of the tibia and polydactyly (E) and unlike the Cu mutation, polydactyly on the forelimb (F). Strong ectopic expression of *Shh* (M) and *Ptc* (N) are observed (highlighted with arrows). Scale bars = 500 μ m in (B) and (C); 1mm in (D), (E) and (F); 100 μ m in (G) to (N).

Figure 2. Insertion mutations disrupt limb development to generate an unusual skeletal phenotype. The position of the adenosine insertions are shown (A) adjacent to the WMS site to create the +A and the +AA mutations. The skeletal features of the +A hindlimb in (B) show a triphalangeal digit 1 (arrowhead). (C) shows expression of *Shh* at E11.5 in the

hindlimb of +A mutant. Forelimb of the +AA mutant in (D) shows fusion and duplication of internal digits (asterisks) while the hindlimb in (E) shows bifurcation at the tip of the extra preaxial digit (arrowheads) and the centrally located extra digit (arrow). (F) shows the bending of the hindlimb caused by a shortening of the tibia. The E11.5 WMS+AA hindlimb bud in (G) shows expression of *Shh* along the entire distal edge (black arrowheads). Scale bars = 500µm in (B), (D) and (E); 100µm in (C) and (G); 1mm in (F).

Figure 3. Mutational analysis of the Ebox and the Hx sites in the ZRS. The ZRS (yellow rectangle) is depicted in (A) and the relative locations of the WMS site, the Ebox and the Hx mutation are indicated. Boxes highlight the relative positions of the sequences shown in (Ebox, B) and (Hx, J) respectively. Linking these two regions, the position of the 3'Δ127 deletion is also shown. The gRNA sequences are boxed in the wildtype sequences in (B and J) with the PAM site (in italics). In (B) the EBox (highlighted in blue font) and the deleted nucleotides for each mutation are shown and the numbers of the homozygous animals analysed are indicated below each mutation (as *n*=). Representative fore limb (C) and hind limb (D) from an EboxΔ17 homozygote demonstrate no detectable deviation from wildtype. The *Shh* expression in hind limbs at E11.5 for the wildtype (E), and EboxΔ3 (F), EboxΔ17 (G), EboxΔ16 (H), EboxΔ8 (I) homozygotes are depicted showing a normal pattern of expression. The mutant sequence affected by the 3' deletions near Hx are shown in (J). The wildtype sequence with the position of the Hx mutation (the red base and box) is indicated. The position of Hoxsite 4 is highlighted in orange. The sequences of all the deletions are shown below and the numbers of the homozygous animals analysed are indicated below each mutation (as *n*=). The apparent unaffected fore limb (J) and hind limb (K) of the large 3'Δ127deletion are shown and The levels of expression of *Shh* at E11.5 hind

limb buds shown by in situ hybridization (M) and by quantification by qRT-PCR (N) in 3'Δ127 homozygous embryos. Scale bars = 500μm in (C), (D), (K) and (L); 100μm in (C) – (I) and (M).

665

Figure 4. Deletions near the WMS site reduce the levels of *Shh* expression. (A) The three deletions WMSΔ20, WMSΔ48 and WMSΔ110 are shown relative to the WMS (green line), Ebox sites (blue line) and Hx mutation (red) within the ZRS (yellow rectangle). The homozygous WMSΔ20 mutants are shown in (B, C and H). No limb abnormalities are detected in the forelimb (B) or the hind limb (C). WMSΔ48 limbs are shown in (D) and (E). The forelimb (D) shows loss of a digit and two terminal phalanges on the adjacent digit (arrowheads) and the hindlimb in (G) shows partial loss of digit 3 (arrow). Loss of the middle digit in forelimb (F) and hind limb (G) are shown in the WMSΔ110 deletion. H-K shows *Shh* expression at E11.5 in the hindlimbs of WMSΔ20 (H), WMSΔ48 (I), WMSΔ110 (J) and wildtype (K) embryos. (L) shows the outcome of the quantification by qRT-PCR of *Shh* expression in E11.5 limb buds from wildtype and WMSΔ20, WMSΔ48 and WMSΔ110 homozygous embryos. WMSΔ48 and WMS110 expression levels are significantly ($p < 0.001$) lower than wildtype (Kruskal-Wallis test with Dunn's multiple comparisons). Scale bars = 1mm in (B) and (C); 500μm in (D)- (G); 100μm in (H) - (K).

680

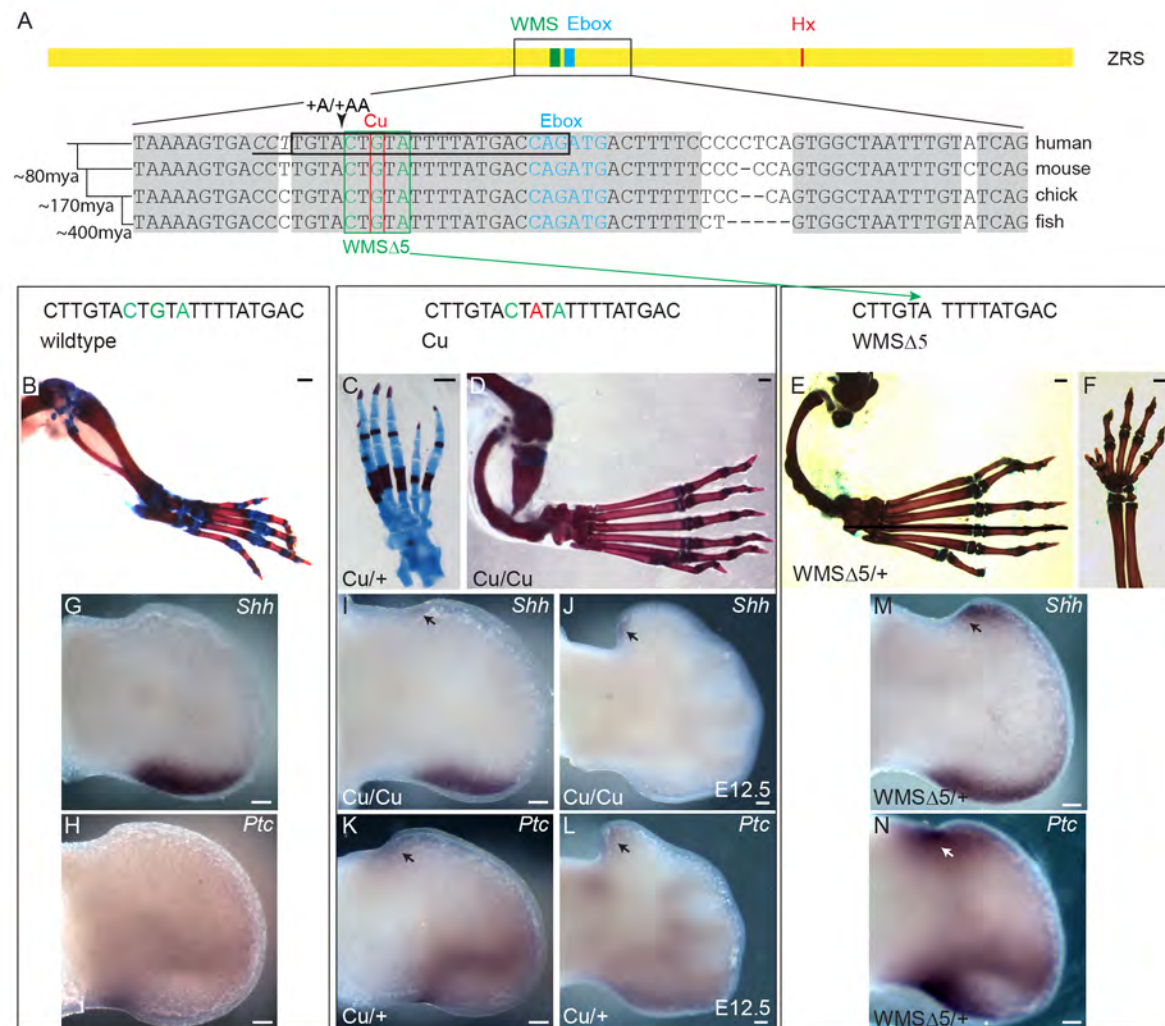
Figure 5. HoxD binding to conserved motifs in the ZRS. The top line shows the genomic sequence round the 4 Hox binding sites (designated Hoxsites1-4), with the position of the WMS region indicated. Also the relative positions of the WMSΔ20, WMSΔ48 and WMSΔ110 deletions are indicated. Below, the sequence of the 4 Hoxsites are shown in the same orientation. The consensus binding sites for each of the proteins HOXD9, D10 and D11 are shown as position weight matrices under their gene names. For each triplet of EMSAs,

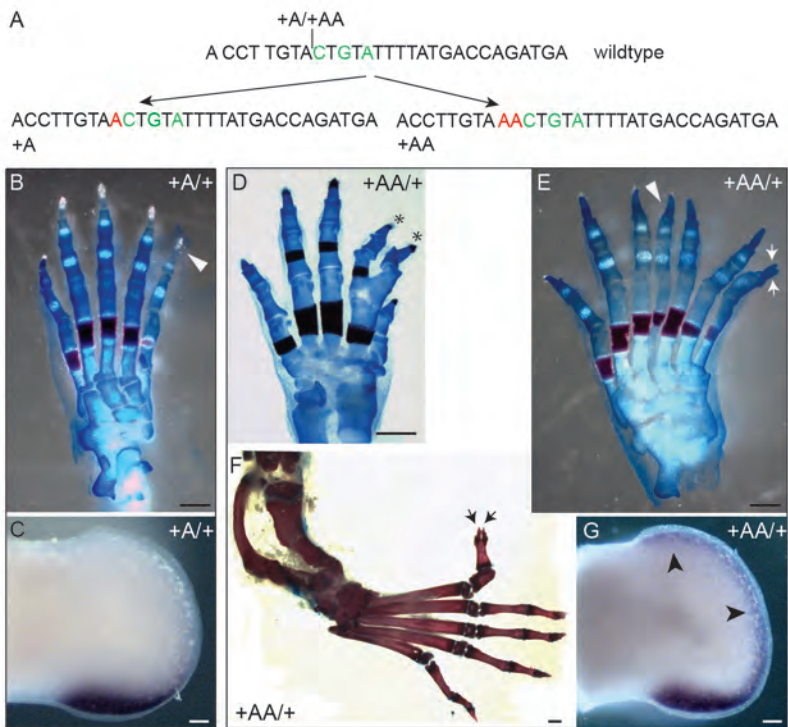
the lanes are shown as binding to a labelled Hoxsite oligonucleotide with no competition, with excess of the wildtype oligo as competitor and with the mutated Hoxsite oligo in competition to show specificity of binding to the Hoxsite. The specific binding is indicated by the arrowheads. In the case of the E11.5 limb bud extract binding to Hoxsite2 a higher mobility shift is observed, indicated by the asterisk. The non-specific band (arrow) is marked as a comparison with Fig S2.

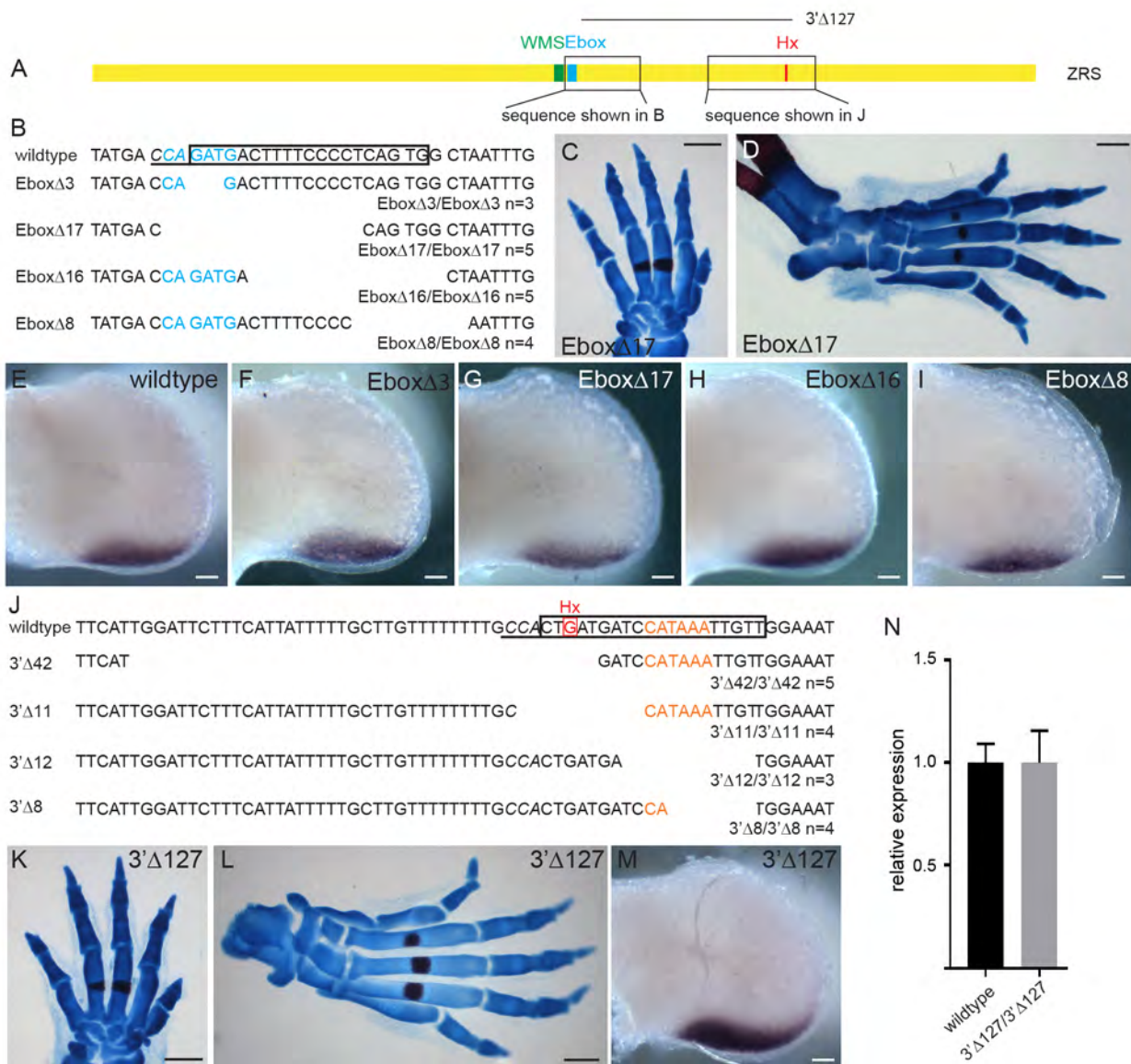
Figure 6. Transgenic analysis of embryos carrying mutant ZRS sequences. (A) shows the sequences of the wildtype Hoxsites 1-3 and the mutated sequences (designated MutHoxsite) that were used in the transgenic constructs. (B-E) Limb buds from transgenic embryos (E11.5) carrying the following ZRS sequences driving LacZ expression: (B) the wildtype ZRS sequences while C-E show the no effect on expression of mutating the Hoxsites singly, MutHoxsite 1 (C), MutHoxsite 2 (D) and MutHoxsite 3 (E). Mutating combinations of sites results in lower LacZ expression; MutHoxsite2+3 shown in (F), MutHoxsite1+3 in (G) and MutHoxsite1,2 +3 in (H). The low level of expression in MutHoxsite1, 2 +3 is reproduced in the WMSΔ110 construct (I). Addition of the Cu point mutation (J) or deletion of the WMSΔ5 (K) results in distal and ectopic anterior expression; whereas, deletion of WMSΔ20 (L) returns expression to wildtype levels. M-O show the Cu mutation in combination with mutant Hox sites; MutHoxsite3+Cu (M), MutHoxsite2+Cu (N) and MutHoxsite2+3+Cu (O). (P) Graphical representation of the LacZ expression patterns resulting from mutations within the ZRS. The width of the expression domain was divided by the width of the limb and expressed as a percentage. One spot represents the extent of reporter gene (*LacZ*) expression for each individual limb from a set of transient transgenic embryos. Data was subjected to a one-way ANOVA and TukeyHSD test and those that differ

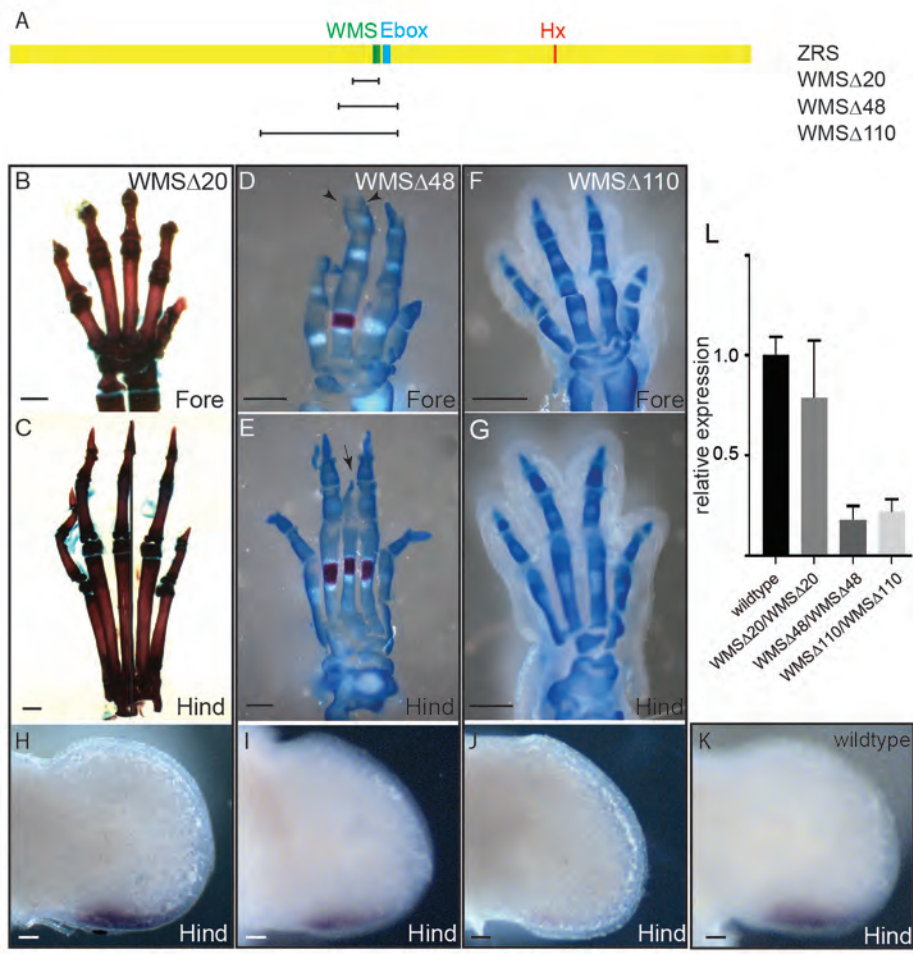
significantly from wildtype are indicated. (* $P \leq 0.05$, *** $P \leq 0.001$, **** $P \leq 0.0001$) Scale bars = 100 μ m.

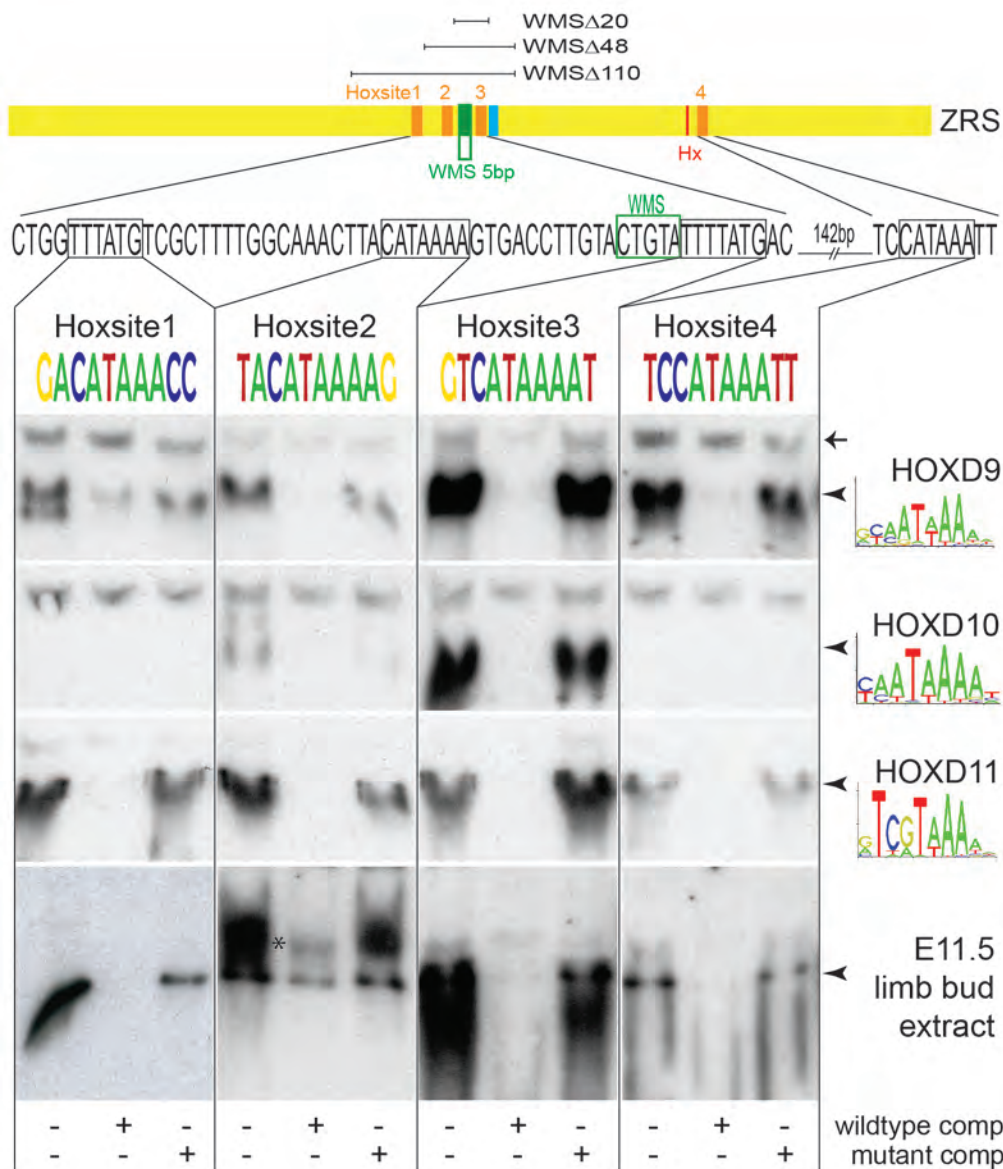
Figure7. A representation of different functional regions and sites established for the ZRS is depicted in (A). The ZRS is represented by the yellow rectangle and the position of the WMS 5bp site (green), the Ebox (blue), the Hx mutations (red) and Hoxsites (orange) are indicated in the ZRS. The positions of the 5 ETS sites that control the position of the expression boundary are represented by the red ovals. The region that contributes to regulating levels is in the blue box and the deletions that revealed this activity are shown. The region that mediates long range activity is shown in the black box. The large region of this domain that is redundant is shown by the grey shading. The two systems that control posterior restriction are shown below the ZRS rectangle indicating the position of the two ETV binding sites and the position of the WMS 5bp site. (B) summarises the positive feedback loop between the 5' *HoxD* genes and *Shh* to reinforce expression of *Shh*. ZRS (yellow box) and its position relative to *Shh* is shown on the left hand side, while a schematic of the HoxD complex including the two flanking regulatory domains (the early enhancer and the late enhancer) is depicted by green boxes on the right hand side. Early expressing 5'HOXD proteins bind Hoxsite 1-3 within the ZRS to establish the levels of *Shh* expression in the initial stages of limb development (arrow 1). The levels of *Shh* expression is dependent on the number of Hox sites occupied. SHH, in turn, is crucial for the shift in HoxD gene expression to the later genes, in particular *Hoxd13* (arrow 2). HOXD13 subsequently binds to sites at the 5' end of the ZRS established by Leal and Cohn (2016) (arrow 3) to maintain *Shh* expression later in limb development.

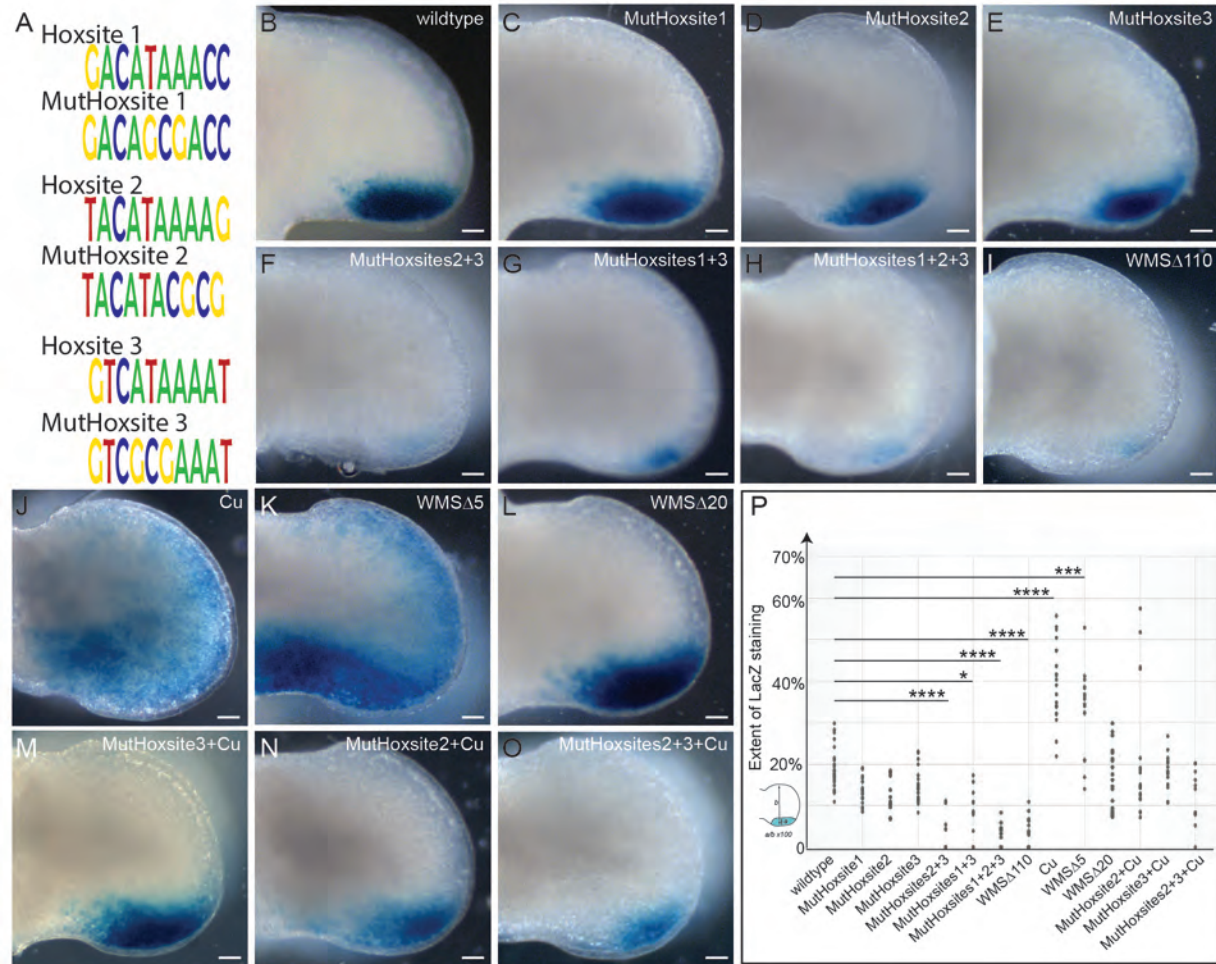












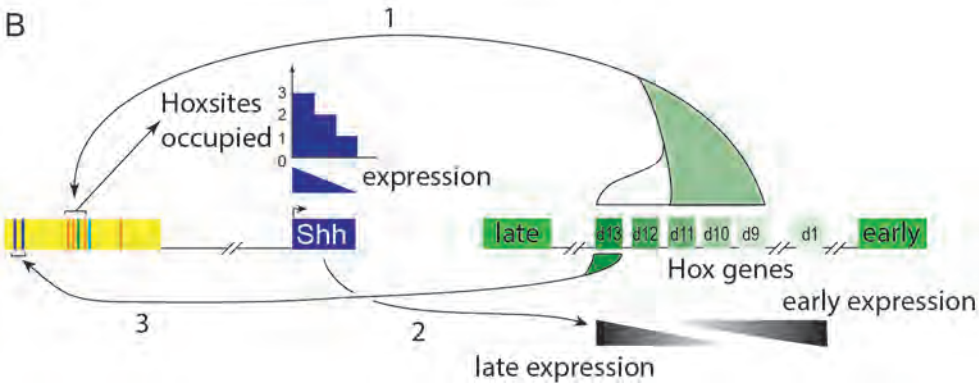
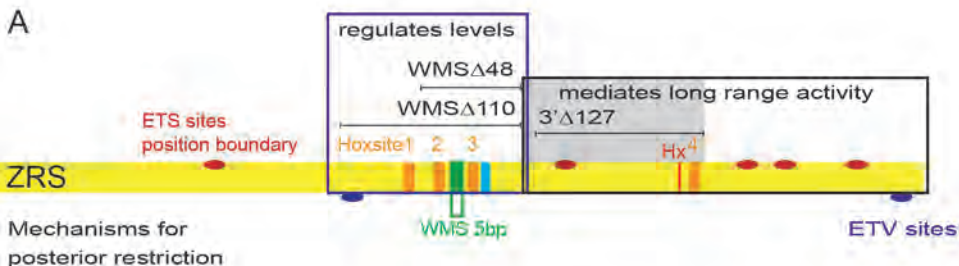


Table S1- Relates to Figures 5 and 6
Oligonucleotides used.

Px330 oligos	
WMS guideF	CACCGTGGTCATAAAATACAGTACA
WMS guideR	AAACTGTACTGTATTTTATGTCCAC
EBox guideF	CACCGCACTGAGGGGAAAAGTCATC
EBox guideR	AAACGATGACTTTTCCCCTCAGTGC
3' guideF	CACCGAACAATTTATGGATCATCAG
3' guideR	AAACCTGATGATCCATAAATTGTTC
Hox gene IVT constructs	
HoxD9F	CATGAT CATATG TCGTCCAGTGGCACCC
HoxD9R	CATGAT CTCGAG GTCTCCTTTAGGGCACTTCTC
HoxD10F	CATGAT CATATG TCCTTTCCCAACAGCTCTC
HoxD10R	CATGAT CTCGAG AGAAAAGGTGAGGTTGGCGGTC
HoxD11F	CATGAT CATATG AACGACTTTGACGAGTGCG
HoxD11R	CATGAT CTCGAG AAATAAGGGGTTTCCAGTGAAATATTG
HoxD12F	CATGAT CATATG TGTGAGCGCAGTCTCTAC
HoxD12R	CATGAT CTCGAG ATAGAGGGCCAGTGCTTGCTC
HoxD13F	CATGAT CATATG AGCCGCTCGGGACTTGG
HoxD13R	CATGAT CTCGAG GGAGACAGTGTCTTTGAGCTTG
Hoxsites EMSA oligos	
Hoxsite 1F	TTGTCCTGGT TTATG TCGCTTTTG
Hoxsite 1R	CAAAAGCGAC CATAA ACCAGGACAA
MutHoxsite 1F	TTGTCCTGGT TgcgG TCGCTTTTG
MutHoxsite 1R	CAAAAGCGA Ccgca ACCAGGACAA
Hoxsite 2F	CAAAC TTACATAA AGTGACCTTGT
Hoxsite 2R	ACAAGGTCAC TTTTATG TAAGTTTG
MutHoxsite 2F	CAAAC TTACATAcgcG TGACCTTGT
MutHoxsite 2R	ACAAGGTCAC CgcgTATG TAAGTTTG
Hoxsite 3F	TGTACTGTAT TTTTATG ACCAGATGACT
Hoxsite 3R	AGTCATCTGGT CATAA AATACAGTACA
MutHoxsite 3F	TGTACTGTAT TTTcgcgG ACCAGATGACT
MutHoxsite 3R	AGTCATCTGGT CgcgAA AATACAGTACA
Hoxsite 4F	CTGATGATCC CATAA ATTGTTGGAA
Hoxsite 4R	TTCCAACA TTTATG GATCATCAG
MutHoxsite 4F	CTGATGATCC CgcgAA TTGTTGGAA
MutHoxsite 4R	TTCCAACA ATTgcgG GATCATCAG
LacZ Transgenic constructs	
ZRS F	GATCATA AAGCTT ACTTTAAGCCATCTTTG
ZRS R	GATCATA AAGCTT CACATAGAACACTTAGTGAG
Mutate ZRS oligos	
Cu F	GACCTTGACT aTATTTTATG ACCAGATGACTTTTCCCTC
Cu R	GAGGGAAAGTCATCTGGT CATAA ATaAGTACAAGGTC
MutHoxsite 1F	CAGTTTGAGATTGTCCTGGT TgcgT GTCGCTTTTGGCAAAC
MutHoxsite 1R	GTTTGCCAAAAGCGAC CAgcgA CCAGGACAATCTCAAAC CTG
MutHoxsite 2F	GTCGCTTTTGGCAAAC TTACATAcgcG TGACCTTGTACTG
MutHoxsite 2R	CAGTACAAGGTCAC gcgTATG TAAGTTTGCCAAAGCGAC
MutHoxsite 3F	GACCTTGACTGTATTT cgcgG ACCAGATGACTTTTCCCTC
MutHoxsite 3R	GAGGGAAAGTCATCTGGT CgcgAA AATACAGTACAAGGTC
MutHoxsite 3F+Cu	GACCTTGACT aTATTTcgcgG ACCAGATGACTTTTCCCTC
MutHoxsite 3R+Cu	GAGGGAAAGTCATCTGGT CgcgAA ATaAGTACAAGGTC

Figure S1-relates to Figure 1

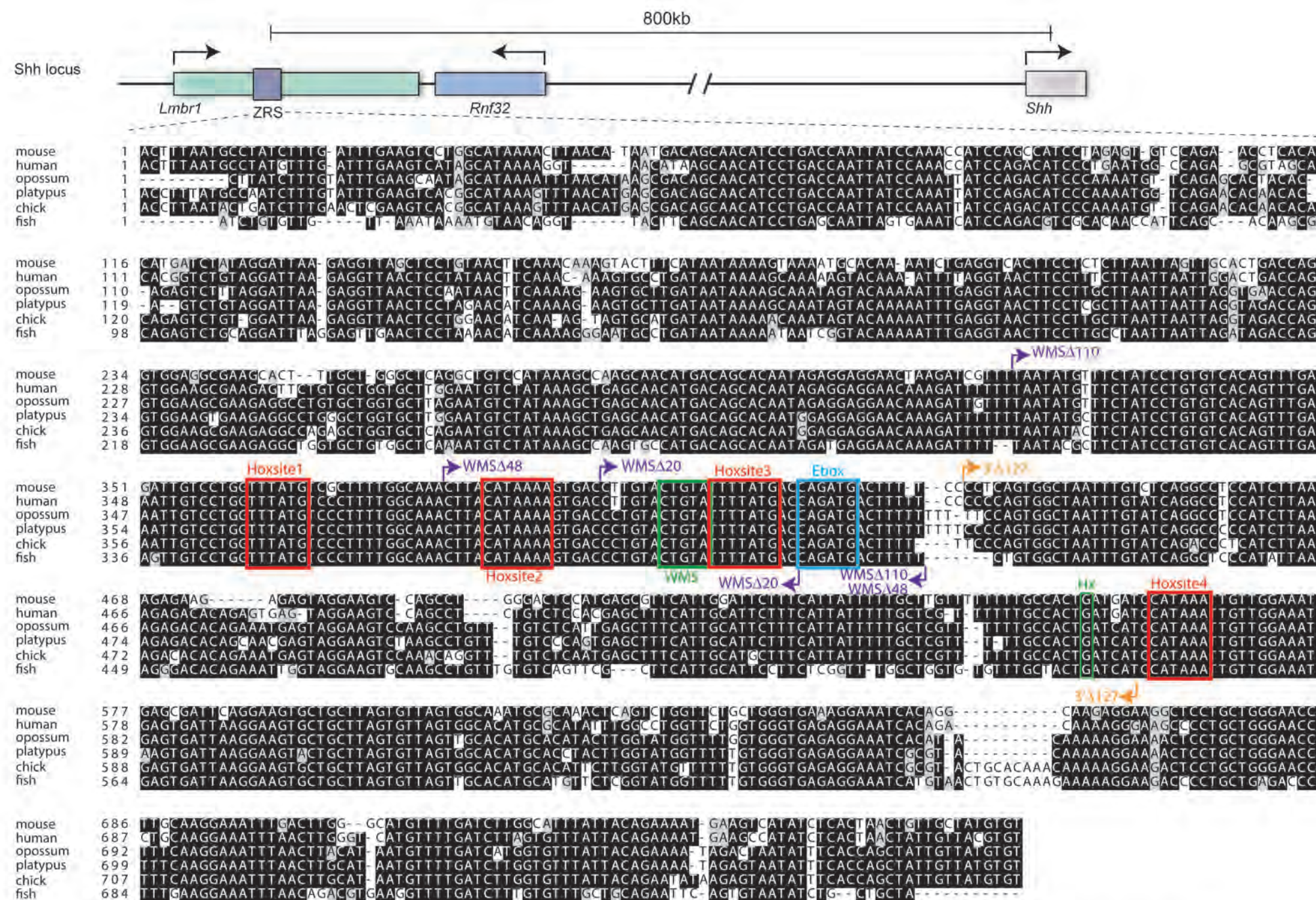
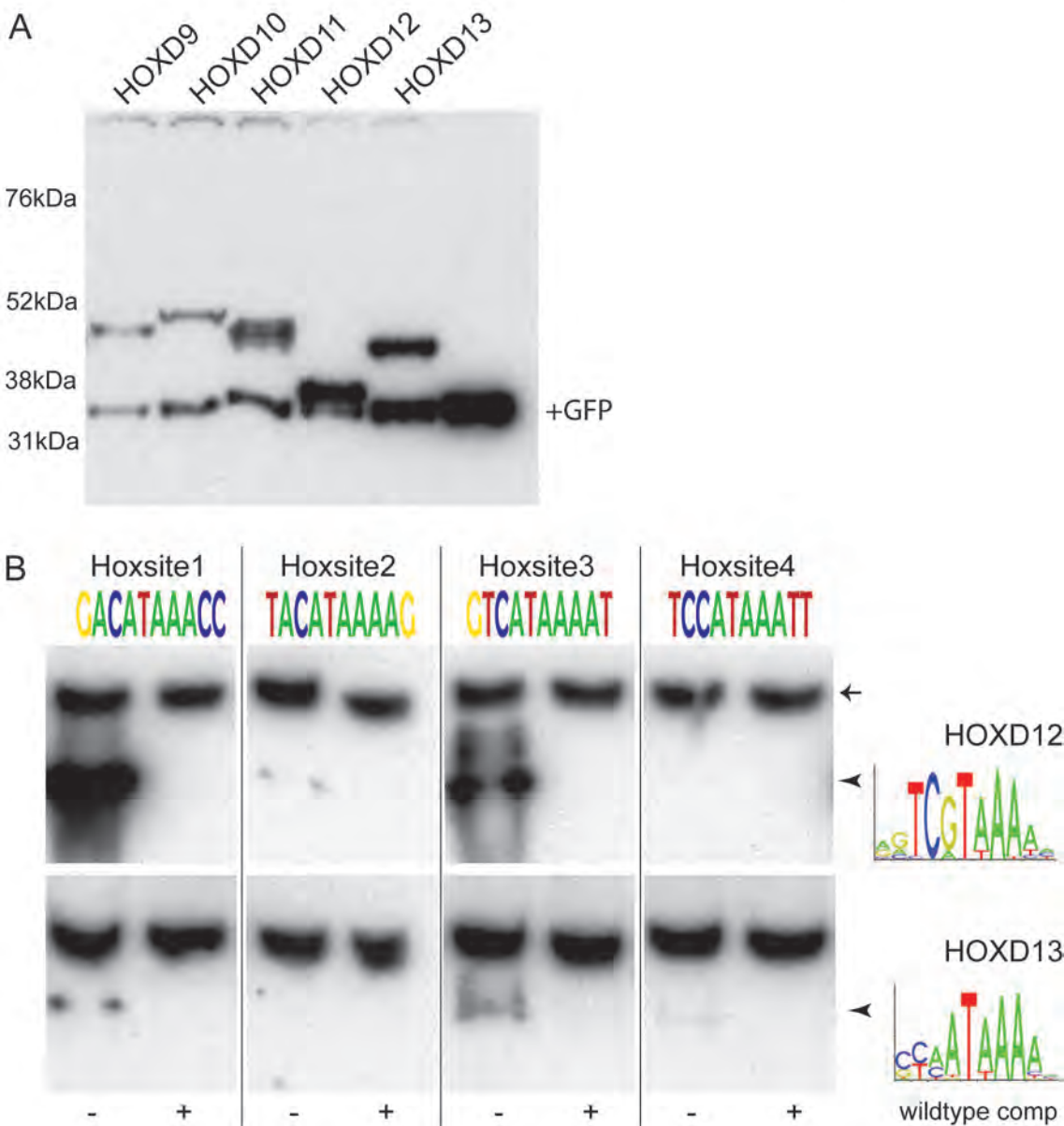


Figure S1. Top line shows a graphical representation of the *Lmbr1* to *Shh* genomic region with the position of ZRS indicated by the grey box. The direction of transcription of the genes is indicated by the arrows. Underneath is the sequence line-up comparing the ZRS in diverse vertebrate species (listed to the left of the sequence) including three different vertebrate classes (mammal, birds and fish) representing >400Myrs of evolution. The sequences for the WMS site and Hx mutation (green) and the Ebox (blue) are boxed. Also boxed in red are the positions of the 4 Hoxsites. The start and end positions of all the large deletions (WMSΔ110, WMSΔ48, WMSΔ20 and 3'Δ127) are indicated.

Figure S2 - relates to Figure 5
Western blots of HOXD proteins and analysis of HOXD12 and D13 binding.



(A) shows a western blot of protein from the IVT reactions probed with an anti HisTag antibody. In addition to the Hox gene containing vector, each reaction included the GFP control vector and a GFP band can be seen in all lanes.

(B) shows the sequence of the Hoxsites1 -4 in the same orientation. The consensus binding sites for the proteins HoxD12 and D13 are shown as position weight matrices under their gene names. For each doublet of EMSAs, the lanes are shown as binding to a labelled Hoxsite oligonucleotide with no competition and with excess of the wildtype oligo as competitor. The specific binding is indicated by the arrowheads, while the non-specific band (arrow) indicates the increased length of exposure time necessary, compare with the equivalent band in Figure 4